Mechatronic Design of a New Robot for Force Control in Minimally Invasive Surgery

Nabil Zemiti, Guillaume Morel, *Member, IEEE*, Tobias Ortmaier, and Nicolas Bonnet

***Abstract*—Minimally invasive surgery (MIS) challenges the surgeon's skills due to his/her separation from the operation area, which can be reached with long instruments only. Therefore, the surgeon looses access to the manipulation forces inside the patient. This reduces his/her dexterity when performing the operation. A new compact and lightweight robot for MIS is presented, which allows for the measurement of manipulation forces. The main advantage of this concept is that no miniaturized force sensor has to be integrated into surgical instruments and inserted into the patient. Rather, outside the patient, a standard sensor is attached to a modified trocar, which allows for the undisturbed measurement of manipulation forces. This approach reduces costs and sterilizability demands. Results of *in vitro* and *in vivo* force control experiments are presented to validate the concepts.**

***Index Terms*—Force control, force measurement, minimally invasive surgery (MIS).**

I. Introduction

THE use of robots for surgical interventions is an approach that is now proven to increase the quality of operations and to establish new types of surgical procedures (see [1] for an up-to-date overview of this research field). Especially, minimally invasive surgery (MIS) in which long instruments are used to access the area of interest seems to be a promising field for robotic surgery. Here, robots help the surgeon to regain virtually direct access to the operation field he/she is separated from: Actuated instruments provide him/her with full dexterity inside the patient as in open surgery. In order to enhance the overall system performances, force control capabilities are desirable [2]. First, they could allow the robot to run in an autonomous force controlled mode, helping to prevent unintentional damage of tissue or to compensate for organ motion in the case of contact between instrument and organ. Additionally, manipulation forces could be displayed back to the surgeon (with appropriate kinesthetic input devices), providing him/her with direct sensation of the remote forces applied to the organ [3].

Unfortunately, currently available minimally invasive robotic surgery (MIRS) systems do not provide any force control. A major obstacle for the development of such a feature lies in the force measurement problem. Indeed, small and sterilizable force sensors, which could be inserted into the patient, are still missing (see Section II for an ongoing research overview). This has motivated our research for the development of a new robot named MC^2E (French acronym for *compact manipulator for endoscopic surgery*).

Apart from its compactness, the main feature of this robot is that it offers a new possibility of force measurement in MIRS. Namely, MC^2E can measure the distal organ–instrument interaction with a sensor placed outside the patient (thus subject to much less sterilization and miniaturization constraints). Remarkably, due to the special mounting of the force sensor, these measurements are not affected by the disturbance forces and torques arising from the interaction between the trocar and the instrument.

The remainder of this paper is organized as follows. Section II gives an overview of researches in the field of force measurement in MIRS. In Section III, MC^2E kinematics is presented. Section IV describes the novel principle of force measurement for MIRS in detail, while Section V provides experimental evidence of this system. Force control and *in vivo* experimental results are then given in Section VI. A discussion of the results and further directions for research are given in Section VII.

II. Related Work

Since the early 1990s, more than 35 surgical robotic systems have been developed [1]. In the field of MIRS especially three commercial systems are to be mentioned: the Zeus system (Computer Motion Inc. [4]), the daVinci system (Intuitive Surgical Inc. [5]), and the Laprotek system (endoVia Medical Inc. [6]). The daVinci system is in clinical use, whereby approximately 150 installations are recorded. The Zeus system was also in clinical use, but is no longer commercially available. Furthermore, the robotic telesurgical workstation for laparoscopy (University of Berkeley, CA, and University of San Francisco, CA) has to be pointed out [7]. None of these systems provides kinesthetic feedback and, thus, prototypical force feedback systems are currently available only at research laboratories. The following provides an overview of research activities in the area of MIRS systems with force measurement and kinesthetic feedback capabilities.

In Korea, a group at Korea Advanced Institute of Science and Technology (KAIST) has developed a telepresence system for microsurgical tasks [8]. It is designed for six-degrees-of-freedom (DoFs) force/torque reflection at the master console. The slave consists of an industrial six-DoFs robot for positioning a modified six DoFs Stewart platform for micromanipulation. The system does not provide full manipulability (i.e., six DoFs)

Manuscript received March 2, 2006; revised May 3, 2006. Recommended by Technical Editor J. P. Desai.

N. Zemiti and G. Morel are with the Laboratoire de Robotique de Paris, Université Pierre et Marie Curie-Paris 6, F-92265 Paris, France (e-mail: zemiti@robot,jussieu.fr; guillaume.morel@upmc.fr).

T. Ortmaier was with the Laboratoire de Robotique de Paris, Université Pierre et Marie Curie-Paris 6, F-92265 Paris, France. He is now with the German Aerospace Center (DLR), 82230 Munich, Germany (e-mail: Tobias.Ortmaier@dlr.de).

N. Bonnet is with the La Pitié Salpêtrière Hospital of Paris, F-75013, France (e-mail: nicolas.bonnet@psl.ap-hop-pairs.fr).

Digital Object Identifier 10.1109/TMECH.2007.892831

for laparoscopic surgery due to the kinematic restrictions at the fulcrum point. Nevertheless, it is one of the few systems, which realizes full force/torque feedback.

In [9], a teleoperated endoscopic grasper for MIS and its experimental evaluation is presented. This system allows for realistic force feedback of endoscopic grasping forces. In an empirical test of ranking the stiffness of silicone materials, the force feedback grasper turned out to be significantly better than a standard laparoscopic grasper, though it was inferior to the performance achieved by the bare hand. However, it is to be mentioned that the experimental setup does neither realize the measurement nor the feedback of contact forces. Besides, the grasper is not fixed to a robot and only one DoF for opening and closing the grasper is available at the moment.

A further approach for measuring grasping forces is addressed in [10]. Here, conventional laparoscopic tools are equipped with strain gauge sensors, and the sensed forces are displayed by a PHANToM (SensAble Technologies Inc.), a rather widespread haptic device. As this tool is also not yet fixed to a robot and the handle is not actuated, the current setup requires two users: one to actuate the surgical instrument and the second one to feel the grasping forces at the PHANToM. At least two further issues have to be mentioned. First, no contact forces can be measured at present. Second, as the strain gauge sensors are placed at the proximal end, the grasping forces are superposed by friction.

A vision-based approach for force sensing is discussed in [11]. Here, an industrial robot (Mitsubishi PA-10) is equipped with a flexible membrane on which artificial landmarks were attached. The positions of the landmarks are tracked by a stereo camera, and the displacements are used to derive the appearing contact forces. Unfortunately, the force feedback update rate is limited to 30 Hz due to the camera frame rate. Besides, it remains open whether this method is sensitive and robust enough for describing the interaction with organic materials.

A force reflecting master–slave system for MIS is described in [12]. In this bilateral system two modified PHANToMs are used: one serves as a force-reflecting master and the other one is equipped with a custom-built instrument and constitutes the slave robot. Master and slave are coupled via virtual-reality peripheral network (VRPN). To control the position of the instrument tip, an artificial neural network is applied, which supports an online adaption to different load conditions at the instrument tip. Unfortunately, here too, the strain gauge sensors are placed at the proximal end, so that the measured contact forces are distorted by the interaction forces between instrument and trocar.

A sensorized and an actuated gripper for MIRS are proposed in [13]. To regain full dexterity (i.e., six DoFs) inside the patient, the setup uses a pair of forceps with two DoFs at the distal end. A custom-made miniaturized force/torque sensor, which is placed close to the gripper, allows for the measurement of contact forces/torques. The sensor has a resolution of about 9 bits, and the sample rate is 900 Hz [14]. Additionally, a propulsion unit is introduced. It is connected mechanically as well as electronically to the robot, and consists of two parts: one part is designed for patient contact and, thus, does not contain any electromechanical or thermo-instable components in order to be steam-sterilizable, whereas the other part integrates all thermo-instable components, like motors and electronics, and for this reason meets only the demand of being spray-sterilizable. The actuated gripper has not yet been integrated into a telesurgery system.

A force feedback telesurgery system is described in [3]. The master consists of a stereo display (25-Hz active stereo with shutter glasses) and a PHANToM serves as an input device. This haptic device provides six DoFs for position and orientation sensing, and uses three translational DoFs for force feedback. The slave is composed of two surgical robots, an Aesop 3000 DS and an Aesop 1000 DS (both from Computer Motion Inc). The Aesop 1000 DS provides a stereo video from the surgical site, as it is equipped with a rigid endoscope. The Aesop 3000 DS is equipped with a sensorized rigid scalpel (thus, four DoFs remain inside the patient). The sensor is placed at the distal end of the instrument, and allows for the measurement of the six components of the manipulation wrench. For details of the sensor, see [14]. Force control experiments with estimation of the (unknown) environment stiffness are presented in [3] and [15].

In [16], a sensorized laparoscopic grasper is presented. The sensor is integrated into the gripper jaws, and measures grasping force (force component normal to the gripper jaws) as well as lateral and longitudinal forces occurring inside the jaws. Unfortunately, the principle of measurement is not explained in detail. The data of the miniaturized sensor are compared to an external load cell as reference sensor. The measurement is supposed to be reliable, as the presented curves for longitudinal forces are similar in shape and the deviation between the curves is marginal. This prototype instrument has not yet been integrated into a robotic surgery system.

In [17], a miniaturized force sensor for hand-held microsurgical instruments or robotic manipulators is presented. The diameter of the sensor is 12.5 mm. The measurement principle is based on bonded silicon strain gauges, which are connected to half-bridges, allowing for the measurement of the three-dimensional force vector. Moments are not sensed. The standard deviation of the force signal, sampled with 100 Hz and fed through a 10-Hz lowpass anti-aliasing filter, is approximately 0.5×10^{-3} N. The authors do not make any remarks on the sterilizability of the sensor.

III. Robot and Kinematics

A robot used in the operating room (OR) has to be lightweight and compact, as only a small amount of space for additional equipment is available. Furthermore, a lightweight robot can be easily mounted and removed by one nurse, which helps to reduce preoperative setup time and is also a safety feature in emergency situations.

In MIS, the instrument has to be moved around an invariant point (fulcrum point), lying on the patient's skin. This point binds two DoFs, and only four DoFs remain inside the patient, if rigid instruments are used, as it is in the case discussed here. This kinematic constraint has to be taken into account by the MIRS system. At least three different designs providing the

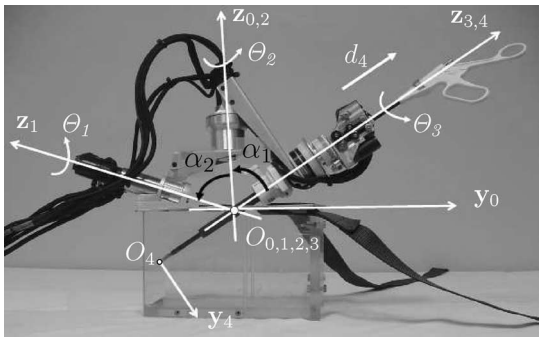

Fig. 1. Photograph of the MC^2E robot, together with coordinate frames and (modified) Denavit–Hartenberg parameters.

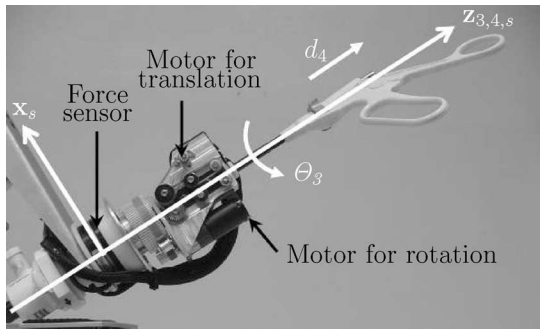

Fig. 2. Upper part of the MC^2E robot, which realizes rotation and translation of the instrument.

limitation or cancellation of the forces exerted on the patient at the fulcrum point can be distinguished.

First, the robot can be equipped with two passive joints at the wrist, in such a way that it frees the orientation of the instrument around the robot end-effector point (see the example of the Zeus robot [4]). As a result, when inserted into the trocar, the instrument naturally rotates around the fulcrum point for any motion of the robot end-effector point. Furthermore, no precise positioning of the robot with respect to the entry point is necessary. Therefore, the setup procedure is facilitated and, thus, operation time is saved. This solution provides a satisfactory behavior as soon as the instrument firmly contacts the trocar. However, in some configurations, a backlash appears between the trocar and the instrument. This leads to a lack of control of instrument motion.

As a second solution, some robots offer a specialized kinematic design dedicated to MIS (e.g., the daVinci system from Intuitive Surgical Inc. [5] and the robotic telesurgical workstation developed by the Universities of California at Berkeley and San Francisco [7]). These robots feature a remote center of rotation, i.e., an invariant point which has to fit the fulcrum point in order to avoid damage to the patient's tissue. As a result, the installation of the MIRS robot base may require a second mechanism for precise positioning, which leads to a rather large system.

Finally, as a third solution, (serial) robots with no "in built" invariant point can be used in MIRS procedures. In this case, an estimation of the fulcrum point location is necessary, as it is to be included in the robot's inverse kinematics. Examples are given in [18], where an end-effector force sensor is used to estimate the entry point position, or in [19] and [20], where the robot joint sensors are exploited.

Unlike most other MIS robots, MC^2E moves not only the instrument but also the trocar in which the instrument is inserted. More precisely, the robot consists of two parts, as shown in Fig. 1. The lower part is a compact spherical two-DoFs mechanism (Θ_1 and Θ_2) at which joint axes coincide with the trocar center. This provides an invariant center at the fulcrum point. The base of this lower subsystem is easily installed on the patient's skin and clipped to the trocar. Once the robot is attached to the trocar, the robot is correctly centered, too (i.e., the fulcrum point on the patient's skin and the invariant point of the robot coincide). This eases the installation of the system and reduces the necessary setup time. The upper part of the robot (Fig. 2) is mounted on the trocar. It provides the two remaining DoFs: the rotation about the instrument axis (Θ_3) and translation along the instrument axis (d_4). In order to translate the instrument along its penetration axis, the motor rotational motion is transmitted through six soft rollers that press the instrument surface (see Fig. 2). This participates in the design compactness, as this system can realize an arbitrarily large translation while remaining rather small.

TABLE I
MAXIMAL DIMENSIONS OF MC^2E

max	configuration	value
height	$\Theta_1 = 60°$, $\Theta_2 = 100°$	19 cm
width	$\Theta_1 = 0°$, $\Theta_2 = 0°$	36 cm
breadth	$\Theta_1 = 0°$, $\Theta_2 = 90°$	20 cm

As observed in Fig. 1, the design is rather compact (see Table I for dimensions of MC^2E, without instrument inserted) and lightweight ($\approx$1.3 kg for the entire robot). Furthermore, it allows for the use of standard disposable instruments, and enables comanipulation by the surgeon and the robot. Note that a similar compact design is proposed in [21] for an endoscope holder. However, in [21], the robot does not include any force measurement feature, and its kinematics suffers from a singularity in the middle of the workspace.

Two different types of motors manufactured by *Faulhaber* were chosen: two powerful motors (2342S024CR series, 12 W) for the spherical part (Θ_1 and Θ_2) of the robot, and two smaller motors (1724T003SR series, 4 W) for the upper part (Θ_3 and d_4) of the robot. With these actuators, the maximum applied force at the instrument tip are $\approx$15 N along the x_4- and y_4-axis and $\approx$8 N along the z_4-axis (beyond this value, the instrument slips within the translating device).

The encoder resolution (512 increments per revolution of the motor) provides, in combination with the gear ratios, sufficient resolution at the link side for high-accuracy motion.

The robot is equipped with a *Nano43* six-axes force/torque sensor manufactured by *ATI Industrial Automation* connected to a 16-bits data acquisition (DAQ) system. Table II summarizes the specifications of this force measurement equipment.

TABLE II
SPECIFICATIONS FOR THE ATI NANO43 FORCE/TORQUE SENSOR

Specification	Value
Force sensing range (x,y,z-axis)	± 36N
Torque sensing range (x,y,z-axis)	± 0.5Nm
Weight	39 g
Diameter (out/in)	43 mm/19.9 mm
Height	11.5 mm
Force resolution (x,y,z-axis)	1/512 N
Torque resolution (x,y,z-axis)	1/40000 Nm

TABLE III
MODIFIED DH PARAMETERS

	α_i	a_i	Θ_i	d_i
$\boldsymbol{T}_{0\to1}$	α_1	0	Θ_1	0
$\boldsymbol{T}_{1\to2}$	$-\alpha_1$	0	Θ_2	0
$\boldsymbol{T}_{2\to3}$	$-\alpha_2$	0	Θ_3	0
$\boldsymbol{T}_{3\to4}$	0	0	0	$-d_4$

The particular mounting is described in detail in Section IV. A sample rate of 670 Hz is used to realize the force control law presented in Section VI.

The modified Denavit–Hartenberg (DH) parameters, shown in Fig. 1 together with the relevant frames, are summarized in Table III.

The overall transformation from the instrument tip frame $\mathcal{F}_4$ to the robot base frame $\mathcal{F}_0$ is

$$\boldsymbol{T}_{0\to4} = \boldsymbol{T}_{0\to1}\boldsymbol{T}_{1\to2}\boldsymbol{T}_{2\to3}\boldsymbol{T}_{3\to4} = \begin{bmatrix} \boldsymbol{R}_{0\to4}^{3\times3} & x \\ 0^T & 1 \end{bmatrix} \quad (1)$$

where $\boldsymbol{T}_{i\to j}$ (resp. $\boldsymbol{T}_{i\to j}$) denotes the homogeneous transform (resp. rotation) from frame $\mathcal{F}_i$ to frame $\mathcal{F}_j$, and x stands for the position of the instrument tip in the robot base frame. Noticing that the angle Θ_3 does not affect the instrument tip position x, one selects the following vector in order to parameterize the four instrument DoFs:

$$\boldsymbol{p} = [x^T(\Theta_1, \Theta_2, d_4), \Theta_3]^T. \quad (2)$$

The kinematic model of the system, which maps the joint velocity vector $[\dot{\Theta}_1, \dot{\Theta}_2, \dot{\Theta}_3, \dot{d}_4]$ to the corresponding twist $[{}^0\mathbf{v}(O_4), {}^0\omega]$ expressed in the robot base frame $\mathcal{F}_0$, is given by

$$\begin{bmatrix} {}^0\mathbf{v}(O_4) \\ {}^0\omega \end{bmatrix} = \boldsymbol{J} \begin{bmatrix} \dot{\Theta}_1 \\ \dot{\Theta}_2 \\ \dot{\Theta}_3 \\ \dot{d}_4 \end{bmatrix} \quad (3)$$

where $\boldsymbol{J} \in \mathbb{R}^{6\times4}$ is the Jacobian matrix of the system.

The rank of the Jacobian matrix $\boldsymbol{J}$ is 4 except at robot singularities, when

$$d_4 = 0 \quad (4)$$

$$\Theta_2 = \pm k\pi, \quad \text{with} \quad k = 0, 1, 2, \ldots. \quad (5)$$

The first singularity, which is of second order, is reached when the instrument tip is at the fulcrum point. It has no consequence during experiments. Indeed, it is crossed only when inserting or removing the instrument, which can be done under joint position control. For the second singularity, $\Theta_2 = \pi$ cannot be reached due to joint limits. Thus, the only physically feasible singularity is $\Theta_2 = 0$, which separates the workspace into two parts. During experiments, one initially chooses $\Theta_2 > 0$ or $\Theta_2 < 0$, and the singularity is never crossed. Of course, this reduces the end-effector workspace. However, in [22], where the same two-link spherical kinematic structure is studied (with the same DH parameters, up to a few degrees), it is shown that half of the workspace of the device is sufficient to realize standard surgical procedures. In the remainder of the paper, the angle Θ_3 is considered to be fixed, and only the position x of the instrument tip is controlled.

Fig. 3. Mounting of the trocar, the passive guide, and the force sensor.

IV. FORCE MEASUREMENT

In manual MIS, the surgeon is separated from the operation area, which is reached by long instruments. Manipulation forces can hardly be sensed by the surgeon, due to the friction in the trocar and the torques necessary to rotate the trocar around the fulcrum point [23], [24]. These disturbances may be dominant, e.g., in heart surgery, where the trocar is placed in the narrow space between the ribs. To overcome this problem, surgeons use tissue deformation as a visual substitute for the feeling of manipulation forces, which does not work with stiff materials such as needles and threads. It is expected that force measurement and force feedback in MIRS increase the immersion of the surgeon into the remote side and help to avoid the interpretation of tissue deformation as well as the unintentional damage of needles and threads [2], [3].

Force measurement can be realized by placing miniaturized force/torque sensors near the instrument tip inside the patient [14]. Here, questions of sterilizability and electromagnetic compatibility still need to be answered. On the contrary, if the force sensor is integrated in the instrument shaft and placed outside the patient, disruption in the force measurement occurs due to friction in the trocar and torques necessary to rotate the trocar.

The solution proposed here is a new trocar in which the sensor is integrated, but placed outside the patient, which drastically reduces the sterilization and miniaturization problems. This is possible, as the trocar is moved (and so is the force sensor) to realize motion inside the patient (see Section III).

The mounting of the trocar and the force sensor is depicted in Fig. 3: an ATI *Nano43* force/torque sensor is used. It has a

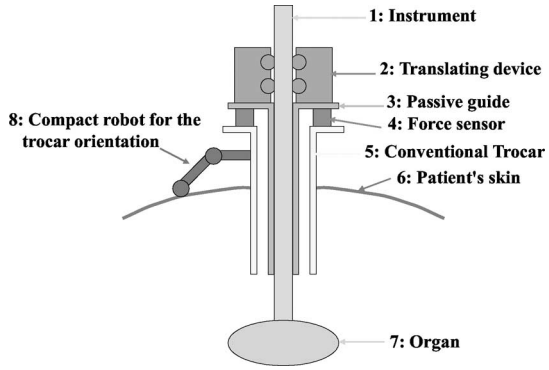

Fig. 4. Modified trocar with integrated force sensor allowing for the measurement of contact forces.

cylindrical shape with a hole at its center. It allows for measuring six components of forces and torques between its top and bottom plate. The bottom plate is attached to a conventional trocar, which includes seals. On the top plate, a passive guide is mounted, with inner seals as well, the axis along which the instrument can translate and rotate. The passive guide penetrates through the sensor hole inside the trocar without any contact with the trocar. Consequently, if the trocar is chosen as the reference body, the sensor measures the wrench applied to the passive guide as detailed in Section IV-A.

A. Force Transmission Model

The setup depicted in Fig. 3 allows for the measurement of the interaction forces between the instrument tip and tissue, without having to cope with friction inside the trocar. The dynamic equation of the instrument (1) states

$$0 = w_{2\to1} + w_{3\to1} + w_{7\to1} + w_{g_1} - w_{d_1} \tag{6}$$

where, in general, w_{g_i} is the wrench applied to part i due to gravity, w_{d_i} is the dynamic wrench of part i, accounting for the inertial effects due to acceleration, and $w_{i\to j}$ denotes the wrench applied by part i to part j. More precisely, accounting for parts numbering depicted in Fig. 4, $w_{2\to1}$ denotes the wrench transmitted by the translating device to the instrument through the rollers, $w_{3\to1}$ denotes the interaction wrench between the instrument and the passive guide, which includes friction due to the relative translation along the penetration axis and the seals, and $w_{1\to7}$ is the interaction wrench of interest (between instrument and organ).

Similarly, the dynamic equations of part (2) and (3) are

$$0 = w_{1\to2} + w_{3\to2} + w_{g_2} - w_{d_2} \tag{7}$$

$$0 = w_{2\to3} + w_{1\to3} + w_{4\to3} + w_{g_3} - w_{d_3}. \tag{8}$$

In these equations, $w_{2\to3}$ is the interaction wrench between the translating device and the passive guide, whereas $w_{4\to3}$ is the wrench measured by the sensor. Summing up (6)–(8) yields

$$w_{1\to7} = w_{4\to3} + w_g - w_d \tag{9}$$

with the sum of wrenches due to gravitation as

$$w_g = w_{g_1} + w_{g_2} + w_{g_3} \tag{10}$$

and the sum of dynamic wrenches as

$$w_d = w_{d_1} + w_{d_2} + w_{d_3}. \tag{11}$$

Remarkably, neither the friction between the instrument and the passive guide, $w_{1\to3}$, nor the wrench between the trocar and the patient's skin, $w_{5\to6}$, influence the measurement. Therefore, there is no need for any model to check these disturbances. Rather, in order to calculate the interaction wrench $w_{1\to7}$, one has to know the gravitation wrench w_g and the dynamic wrench w_d. Usually, $w_d \approx 0$ holds, as velocities and accelerations in MIS are rather small, which leads to

$$w_{1\to7} = w_{4\to3} + w_g. \tag{12}$$

Therefore, in practice, estimating the distal interaction $w_{1\to7}$ from the measured wrench $w_{4\to3}$ is reduced to a gravity compensation algorithm.

B. Gravity Compensation

1) Compensation Algorithm: The equation given in (12) suggests that the interaction wrench $w_{1\to7}$ can be estimated from $w_{4\to3}$ by a simple gravity compensation, which is usually quite straightforward within robot force control. Indeed, the gravitation wrench w_g expressed at the center of gravity G of the parts 1, 2, and 3 of the robot is

$$w_g|_G = [m\boldsymbol{g}, 0_{3\times1}]_G \tag{13}$$

where m denotes the mass of the parts 1, 2, and 3 of the robot, and $\boldsymbol{g}$ denotes the gravity vector with the norm $\|\boldsymbol{g}\| = 9.81\mathrm{N/ms}^{-2}$.

In fact, the wrench measured by the sensor is actually given by

$$w_{\mathrm{mes}} = w_{4\to3} + w_{\mathrm{off}} \tag{14}$$

where $\boldsymbol{w}_{\mathrm{off}} = [\mathbf{f}_{\mathrm{off}}, \mathbf{t}_{\mathrm{off}}]$ is the sensor measurement offset, which corresponds to the measured wrench when the applied wrench is zero (sensor in free load configuration).

Therefore, combining (12)–(14) allows for computing the interaction wrench $\boldsymbol{w}_{1\to7}$ from a gravity model and an offset compensation. More precisely, one can compute this wrench at the center S of the sensor frame $\mathcal{F}_s$, and project the force and torque vectors in the sensor base, which leads to

$$\begin{aligned} {}^s\boldsymbol{w}_{1\to7}|_S &= \begin{bmatrix} {}^s\mathbf{f}_{1\to7} \\ {}^s\mathbf{t}_{1\to7}(S) \end{bmatrix} \\ &= \begin{bmatrix} {}^s\mathbf{f}_{\mathrm{mes}} - {}^s\mathbf{f}_{\mathrm{off}} + \boldsymbol{R}_{s\to0}(m^0\boldsymbol{g}) \\ {}^s\mathbf{t}_{\mathrm{mes}} - {}^s\mathbf{t}_{\mathrm{off}} + [\boldsymbol{R}_{s\to0}(m^0\boldsymbol{g})]_\times {}^s\mathbf{d}_{GS} \end{bmatrix} \end{aligned} \tag{15}$$

where ${}^s\mathbf{f}_{\mathrm{mes}}$ and ${}^s\mathbf{t}_{\mathrm{mes}}$ are the measured force and torque vectors at point S, respectively, ${}^s\boldsymbol{d}_{GS}$ groups the coordinates of the vector from G to S in frame $\mathcal{F}_s$, $\boldsymbol{R}_{s\to0}$ is the rotation from the robot base to the sensor frame which is known from the robot kinematic model, and $[\boldsymbol{a}]_\times$ denotes the skew symmetric matrix associated with a vector $\boldsymbol{a}$ such that, for any vector $\boldsymbol{b}$, $[\boldsymbol{a}]_\times \boldsymbol{b} = \boldsymbol{a} \times \boldsymbol{b}$.

2) Parametric Identification: In order to be able of implementing the compensation algorithm given in (15), it is required to precisely know the offset wrench in the sensor frame, the weight vector $m^0\boldsymbol{g}$ and the position of G in the sensor frame.

In practice, none of these parameters are precisely known in advance. Indeed, we can observe the following.

1) The offset depends on both the preload applied to the sensor and on experimental conditions, such as temperature.
2) Since the robot is placed on the patient at the beginning of the operation, its base has an unknown orientation with respect to a gravitational frame. Thus, the coordinates ${}^0\boldsymbol{g}$ of the gravity vector in the robot base frame are unknown.
3) Since different instruments can be used, both the total mass and the position of G in the sensor frame may vary from an experiment to another.

Therefore, after installing the trocar and the robot, and prior to the operation, a short identification sequence has to be run for each new operation. During this sequence, the robot is placed at several joint configuration to provide a rotation of the instrument around the trocar while contacts between the instrument and organs (or any external environment) are avoided. At each joint configuration, both the joint position and the raw measured wrench are recorded. They are then fed to an identification algorithm.

In practice, avoiding contacts between the instrument and organs can be easily obtained by limiting the instrument penetration d_4 in such a way that the instrument tip remains far away from the organ. Note that in all the joint configurations used for the identification, one has $\boldsymbol{w}_{1\to 7}=0$, even though the instrument penetrate the patient skin.

Thus, introducing subscript i to denote the ith joint configuration in which the wrench is measured during the identification procedure, (15) can be written as

$$\begin{bmatrix} {}^s\mathbf{f}_{\mathrm{mes},i} \\ {}^s\mathbf{t}_{\mathrm{mes},i} \end{bmatrix} = \begin{bmatrix} {}^s\mathbf{f}_{\mathrm{off}} - \boldsymbol{R}_{s\to 0,i}(m^0\boldsymbol{g}) \\ {}^s\mathbf{t}_{\mathrm{off}} - [\boldsymbol{R}_{s\to 0,i}(m^0\boldsymbol{g})]_\times {}^s\boldsymbol{d}_{GS,i} \end{bmatrix}. \tag{16}$$

Considering first the force vector equation, one then has

$${}^s\mathbf{f}_{\mathrm{mes},i} = \boldsymbol{A}_i \begin{bmatrix} {}^s\mathbf{f}_{\mathrm{off}} \\ m^0\boldsymbol{g} \end{bmatrix}, \quad \text{with} \quad \boldsymbol{A}_i = [\boldsymbol{I}_3 - \boldsymbol{R}_{s\to 0,i}] \tag{17}$$

where matrix $\boldsymbol{A}_i$ is known for each joint configuration from the robot kinematic model. Thus, grouping n measured forces into a vector $\mathbf{F}_{\mathrm{mes}} = [{}^s\mathbf{f}_{\mathrm{mes},1}^T \cdots {}^s\mathbf{f}_{\mathrm{mes},n}^T]^T$ leads to the linear equation

$$\mathbf{F}_{\mathrm{mes}} = \boldsymbol{A} \begin{bmatrix} {}^s\mathbf{f}_{\mathrm{off}} \\ m^0\boldsymbol{g} \end{bmatrix} \tag{18}$$

with $\boldsymbol{A} = [\boldsymbol{A}_1^T \cdots \boldsymbol{A}_n^T]^T$. Then, the unknown parameters ${}^s\mathbf{f}_{\mathrm{off}}$, and $m^0\boldsymbol{g}$ can be estimated by a simple least square solution as

$$\begin{bmatrix} \widehat{{}^s\mathbf{f}_{\mathrm{off}}} \\ \widehat{m^0\boldsymbol{g}} \end{bmatrix} = \boldsymbol{A}^+\mathbf{F}_{\mathrm{mes}} = (\boldsymbol{A}\boldsymbol{A}^T)^{-1}\boldsymbol{A}^T\mathbf{F}_{\mathrm{mes}}. \tag{19}$$

In a second step, the torque vector equation in (16) is used for the identification of the remaining parameters. In order to allow for a simple linear identification, the penetration translation d_4 is kept constant ($d_4 = d_{4_0}$) during the identification procedure. Therefore, the center of gravity G for parts 1, 2, and 3 is immobile and constantly coincides with an unknown point G_0. In other words, the vector ${}^s\mathbf{d}_{GS,i} = {}^s\mathbf{d}_{G_0S}$ is constant. Assuming a perfect identification for $\widehat{m^0\boldsymbol{g}}$ from (19), the second line of (16) can then be written as

$${}^s\mathbf{t}_{\mathrm{mes},i} = \boldsymbol{B}_i \begin{bmatrix} {}^s\mathbf{t}_{\mathrm{off}} \\ {}^s\mathbf{d}_{G_0S} \end{bmatrix}, \text{ with } \boldsymbol{B}_i = \Big[\boldsymbol{I}_3 - \Big[\boldsymbol{R}_{s\to 0,i}(\widehat{m^0\boldsymbol{g}})\Big]_\times\Big]. \tag{20}$$

Again, grouping the measured torque vectors into the vector $\mathbf{T}_{\mathrm{mes}} = [{}^s\mathbf{t}_{\mathrm{mes},1}^T \cdots {}^s\mathbf{t}_{\mathrm{mes},n}^T]^T$ and the matrices $\boldsymbol{B}_i$ into the matrix $\boldsymbol{B} = [\boldsymbol{B}_1^T \cdots \boldsymbol{B}_n^T]^T$ leads to the following estimator:

$$\begin{bmatrix} \widehat{{}^s\mathbf{t}_{\mathrm{off}}} \\ \widehat{{}^s\mathbf{d}_{G_0S}} \end{bmatrix} = \boldsymbol{B}^+\mathbf{T}_{\mathrm{mes}} = (\boldsymbol{B}\boldsymbol{B}^T)^{-1}\boldsymbol{B}^T\mathbf{T}_{\mathrm{mes}}. \tag{21}$$

It then remains to estimate the position vector $\widehat{{}^s\mathbf{d}_{GS}}$ when G differs from G_0, i.e., when the translation d_4 of the instrument (1) differs from the value d_{4_0} it had during the identification procedure. To do so, one first distinguishes between the mass m_1 of the instrument, which is supposed to be known (easily measurable in advance) and the mass $m_{2,3}$ of parts 2 and 3. One then has

$${}^s\mathbf{d}_{GS} = \frac{m_1\,{}^s\mathbf{d}_{G^1S} + m_{2,3}\,{}^s\mathbf{d}_{G^{2,3}S}}{m} \tag{22}$$

where G^1 is the center of gravity of the instrument (part 1), $G^{2,3}$ is the center of gravity of the parts 2 and 3, which is independent from d_4, and $\mathbf{d}_{G^xS}$ is the vector from G^x to S. Furthermore, due to the translational displacement along $\boldsymbol{z}_s$ of the instrument from d_{4_0} to d_4, one has

$${}^s\mathbf{d}_{G^1S} = (d_{4_0} - d_4)\,{}^s\mathbf{m}\boldsymbol{z}_s + {}^s\mathbf{d}_{G_0^1S} \tag{23}$$

where ${}^s\mathbf{d}_{G_0^1S}$ denotes the vector from the position G_0^1 of the instrument center of gravity during the identification procedure to the sensor frame center S.

Combining (22) and (23) gives

$${}^s\mathbf{d}_{GS} = \underbrace{\frac{m_1\,{}^s\mathbf{d}_{G_0^1S} + m_{2,3}\,{}^s\mathbf{d}_{G^{2,3}S}}{m}}_{{}^s\mathbf{d}_{G_0S}} - \frac{m_1(d_{4_0} - d_4)}{m}\,{}^s\boldsymbol{z}_s. \tag{24}$$

Therefore, the estimation of ${}^s\mathbf{d}_{GS}$ for an arbitrary value of d_4 is

$$\widehat{{}^s\mathbf{d}_{GS}} = \widehat{{}^s\mathbf{d}_{G_0S}} + \frac{m_1(d_{4_0} - d_4)}{\widehat{m}}\,{}^s\boldsymbol{z}_s \tag{25}$$

where the estimated mass $\widehat{m}$ for parts 1, 2, and 3 can be easily obtained by

$$\widehat{m} = \frac{\|(\widehat{m^0\boldsymbol{g}})\|_2}{9.81\ \mathrm{ms}^{-2}}. \tag{26}$$

V. Experimental Validation of the Measurement Model

A. Validation of the Gravity Compensation

The identification procedure is experimentally performed to verify the quality of the gravity compensation stage. First, the robot is placed at $n = 37$ positions covering the workspace, defined by

$$\Theta_{1,i} \quad \text{and} \quad \Theta_{2,i} \quad \text{and} \quad d_{4,i} = d_{4_0} = 0, \quad \text{with} \quad i = 1, \ldots, n.$$

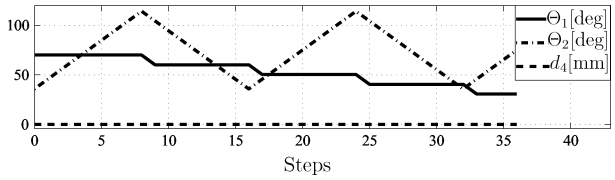

Fig. 5. Joint positions Θ_1, Θ_2, and d_4 used for the robot calibration.

where $\Theta_{1,i}, \Theta_{2,i}$ and $d_{4,i}$ are plotted in Fig. 5. At each position, the sensor forces ${}^s\mathbf{f}_{\mathrm{mes,i}}$ and torques ${}^s\mathbf{t}_{\mathrm{mes,i}}$ are recorded. During the identification, the instrument does not touch the environment, and the wrench is measured while the robot stays still (i.e., $\boldsymbol{w}_d = 0$). The total duration of the identification procedure is approximately 3 min.

The unknown parameters are then estimated according to (19), (21), (25) and (26). The resulting estimated parameters are

$$\widehat{{}^s\mathbf{f}_{\mathrm{off}}} = \begin{bmatrix} 0.64 \\ 2.8 \\ 1.28 \end{bmatrix} (\mathrm{N}) \quad \widehat{{}^s\mathbf{t}_{\mathrm{off}}} = \begin{bmatrix} -111 \\ 24.1 \\ 4.1 \end{bmatrix} (\mathrm{mN{\cdot}m})$$

$$\widehat{{}^0\boldsymbol{g}} = \begin{bmatrix} 0.0 \\ -0.66 \\ -9.79 \end{bmatrix} (\mathrm{N{\cdot}m{\cdot}s^{-2}}) \quad \widehat{m} = 0.373\mathrm{kg}$$

$$\widehat{{}^s\mathbf{d}_{G_0S}} = \begin{bmatrix} -1.44 \\ 4.42 \\ 42.2 \end{bmatrix} (\mathrm{mm}).$$

During the experiment, the robot is placed on an approximately horizontal table, thus, the estimated gravity field vector ${}^0\boldsymbol{g}$ is expected to be close to $\boldsymbol{g}_{\mathrm{th}} = [0, 0, -9.81\mathrm{N/kg}]^T$. Actually, a small angle equal to 3° is experimentally observed between the theoretical value of ${}^0\boldsymbol{g}$ and its estimated value. Next, in order to verify the quality of the estimation, the robot is placed at 23 different locations across the workspace (different from the ones used in the identification), with d_4 varying, while avoiding contacts. Equation (15) is then used to compensate for gravity.

Fig. 6 compares the raw sensor data $({}^s\mathbf{f}_{\mathrm{mes}}, {}^s\mathbf{t}_{\mathrm{mes}}(S))$ and the calculated compensation for each position.

One can observe in Fig. 6 that the error $\boldsymbol{e}$ between the measured and the calculated forces and torques is rather small (less than 0.2 N for the forces and less than 8 mN·m for the torques).

B. Insensitivity of the Measurement to Trocar Disturbances

To validate the force transmission model detailed in Section IV-A, the experiments presented next are performed using an additional external force/torque sensor. In the rest of this section, we consider that the gravity effect is well compensated.

1) Insensitivity To Friction Between the Instrument and the Trocar: For this experiment, a spring of stiffness k is placed on the external sensor as shown in Fig. 7(a). The robot is placed in a vertical position [cf. Fig. 7(b)], while the instrument tip firmly contacts the spring.

Meanwhile, the instrument penetration d_4 is servoed to the desired sinusoidal position depicted in Fig. 8(c). Two forces

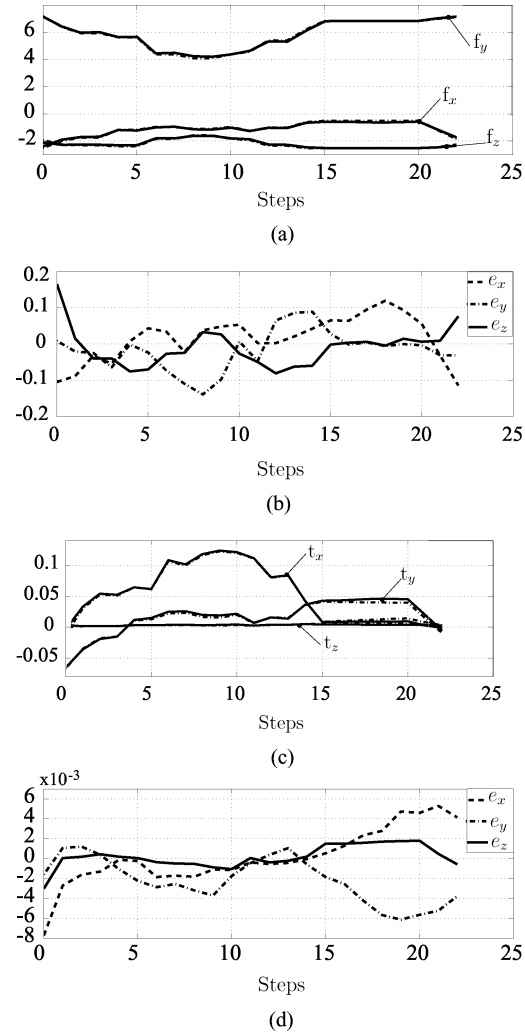

Fig. 6. Calculated and measured forces and torques, together with the estimation errors.

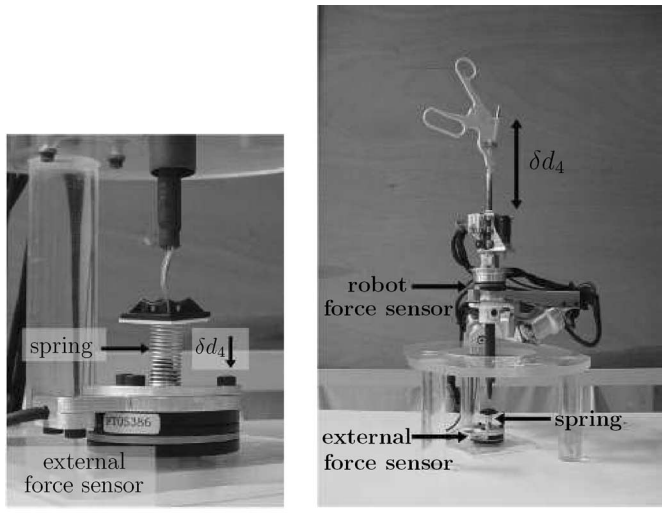

Fig. 7. Experimental setup for the force transmission model validation. (a) Spring placed on the external force sensor. (b) MC^2E applying a force $\mathrm{f} = \mathrm{k}\delta d_4$ on the external force sensor.

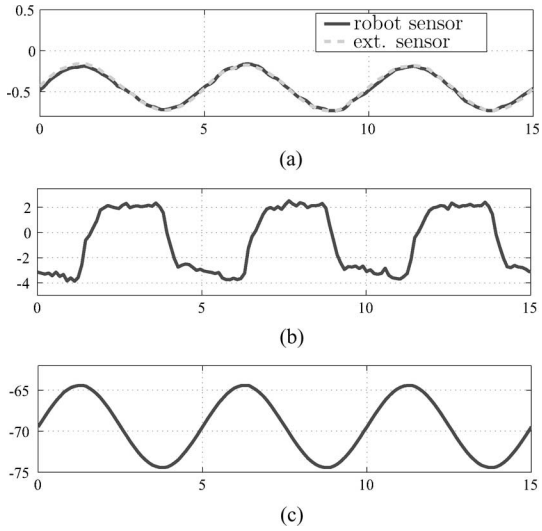

Fig. 8. Measured contact forces from the robot force sensor and from the external force sensor, the computed command force for the translational motor, and the instrument position during the experiment. (a) Force [N] versus time [s]. (b) Command force [N] versus time [s]. (c) Position d_4 [mm] versus time [s].

are then simultaneously measured: one by the external sensor (thus, it corresponds to the effective force at the instrument tip) and one by the robot-mounted sensor, together with the gravity compensation algorithm. During the experiment, as the instrument moves "in and out" in the sealed passive guide, a large amount of dry friction occurs, which changes sign each time the sign of the penetration velocity changes. However, the experimental result, plotted in Fig. 8(a), shows that in spite of this large frictional disturbance, the module of the estimated force (robot sensor) constantly equals the module of the actual force measured by the second sensor (external sensor).

The significance of the amount of friction is illustrated in Fig. 8(b) that plots the equivalent command force produced by the translational motor. This force, which is simply computed from the motor current, drastically varies when the sign of the penetration velocity changes. It reaches approximately 2 N to move the instrument up and approximately -4 N to move it down. These values are large compared to the useful force, which varies between -0.8 and -0.2 N.

One can conclude that the measurement device, which equips the MC^2E robot, allows for the measurement of the contact forces at the distal extremity of the instrument, without being corrupted by the friction between the instrument and the passive guide.

2) Insensitivity to the Trocar–Abdomen Interaction: To evaluate the effect of the trocar–abdomen interaction on the robot force sensor, the setup of Fig. 9 is used.

An artificial abdomen (a piece made of an elastic foam) is pasted on the external sensor, as shown in Fig. 9(a). The trocar is then inserted in the artificial abdomen and clipped to the robot.

During this experiment, the trocar is manipulated around the incision point by servoing the robot joint position Θ_2 to the desired sinusoidal position as reported in Fig. 10(c). Again, one can compare the trocar–abdomen interaction forces (resp. torques) measured by the external sensor to the forces (resp. torques) measured by the robot sensor.

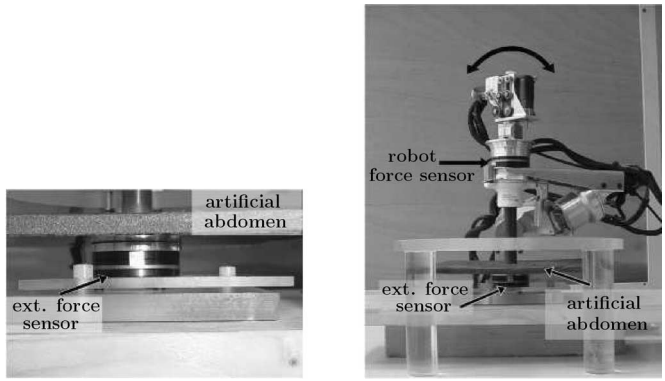

Fig. 9. Experimental setup for the trocar–abdomen interaction evidence. (a) Artificial abdomen pasted on the external force sensor. (b) MC^2E manipulating a trocar inserted in the artificial abdomen.

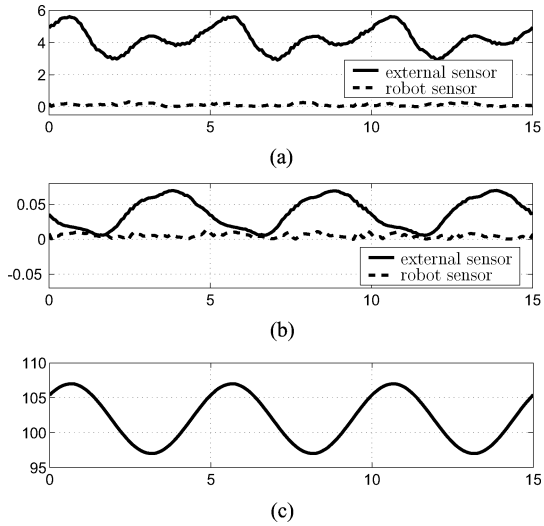

Fig. 10. Measured contact forces and torques from the robot force sensor and from the external force sensor with respect to the joint position Θ_2 during the experiment. (a) Force [N] versus time [s]. (b) Torques [N·m] versus time [s]. (c) Joint position Θ_2 [deg] versus time [s].

The experimental results, given in Fig. 10(a) and (b), show that contrary to the previous experiment, the force (resp. torque) measured by the robot sensor and by the external sensor are not equal. Indeed, as predicted by the measurement model in Section IV, the trocar–abdomen interaction is not measured by the robot-mounted sensor (which measures approximately stay null).

VI. Experimental Results with Force Control

For the force control experiments, the control structure depicted in Fig. 11 is used, where $\boldsymbol{J}$ denotes the robot Jacobian matrix (see Section III) and $\boldsymbol{S}$ a selection matrix.

At the lowest level of the robot controller, a joint torque loop encapsulates the current loop realized in hardware by the power amplifiers. The joint torque controller uses a fixed gain PI compensator with a feedforward compensation.

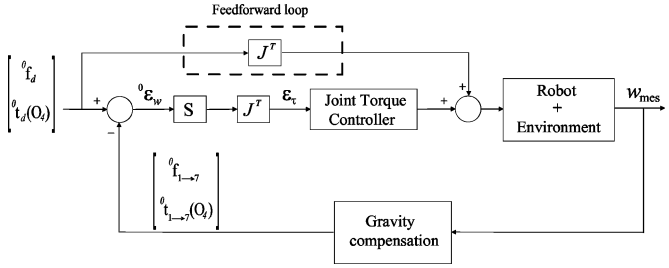

Fig. 11. Control structure used to control the contact forces between instrument and environment.

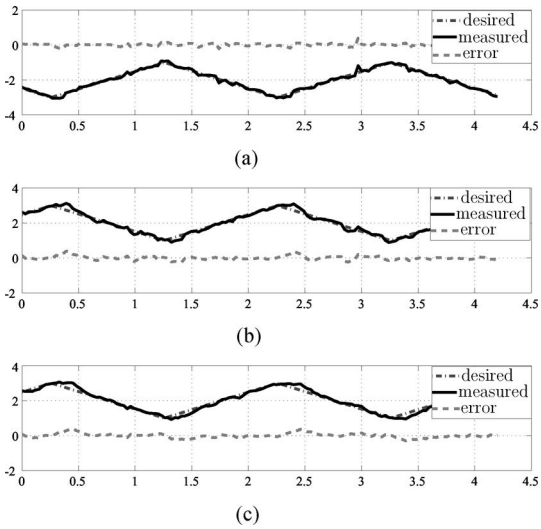

Fig. 12. Trajectories of the desired ($^0\mathbf{f}_d$) and measured ($^0\mathbf{f}_{1\to7}$) contact forces in the robot base frame $\mathcal{F}_0$. (a) Desired and measured contact force ^0f_x [N] versus time [s]. (b) Desired and measured contact force ^0f_y [N] versus time [s]. (c) Desired and measured contact force ^0f_z [N] versus time [s].

In [25], the stability of this controller is investigated using the passivity theory. Necessary and sufficient conditions for the system passivity, applying to both the PI gains (w.r.t. the robot dynamics) and the selection matrix $\boldsymbol{S}$ (w.r.t. the robot kinematics), are formally derived. This analysis provides a formal guarantee that, when a passive environment applies arbitrary forces on the robot end-effector, the system remains stable.

A. Force Response Experiment

Experiments were conducted, where the instrument is rigidly attached to a fixed environment near its tip P, and the desired wrench is set to

$$\begin{bmatrix} {}^0\mathbf{f}_d \\ {}^0\mathbf{t}_d(O_4) \end{bmatrix} = \begin{bmatrix} [f_{x_d} f_{y_d} f_{z_d}]^T \\ [000]^T \end{bmatrix}$$

where f_{x_d}, f_{y_d} and f_{z_d} are triangular signals varying between 1 and 3 N.

The experimental results are given in Fig. 12, where one can observe that the three measured force components are equal to the three desired force components.

The results emphasize the precision of the controller, since the tracking force errors stably remain null. However, this provides no guaranty on the system performance when contacting a soft and moving environment as during real *in vivo* experiments. This is the motivation of Section VI-B.

Fig. 13. MC^2E robot during an *in vivo* laparoscopic cholecystectomy.

B. In Vivo Experiments

A first clinical application of the MC^2E robot was proposed by Dr. Nicolas Bonnet, a surgeon at the La Pitié Salpètriére Hospital of Paris. It consists of replacing the surgeon's left hand by the MC^2E robot during a laparoscopic cholecystectomy (the surgical removal of the gallbladder).

During this operation, MC^2E is equipped with a standard forceps instrument, with manually controlled grasping. In the first stage, MC^2E is servoed to a zero desired force, which allows the surgeon to comanipulate the robot and to grasp the gallbladder. In the second stage, the surgeon pulls the gallbladder with a given force, and MC^2E is frozen. Then, MC^2E is servoed to a constant force, so that it can progressively remove the gallbladder while the surgeon uses an electrocautery knife to detach the gallbladder from the liver. Because of its ability of controlling a constant force, MC^2E can delicately pull the gallbladder and adapt its configuration to the evolving geometry of the operation site. The surgeon can, thus, dissect the gallbladder and manipulate the endoscopic camera and perform the overall operation without the help of any assistant. As shown in Fig. 13, the surgical operation is conducted by only one person, instead of two, as in classical laparoscopic cholecystectomy.

The robot MC^2E's ability of maintaining a constant force, despite physiological movements, is illustrated in the next experiment. The robot is placed on the abdomen of a pig breathing with the help of a medical ventilator, which is a device designed to provide mechanical ventilation to a patient. During this experiment, the robot maintains a small contact force between the instrument tip and the patient's liver. A periodic physiological movement at 0.25 Hz is induced by the medical ventilator and has to be compensated for, in order to maintain contact.

In this situation, the force control scheme depicted in Fig. 11 is used, with the selection matrix $\boldsymbol{S}$ chosen so that only the penetration force is controlled. Consequently, for this experiment, the robot axes Θ_1 and Θ_2 are blocked at a working position, and only the instrument axis d_4 is force controlled

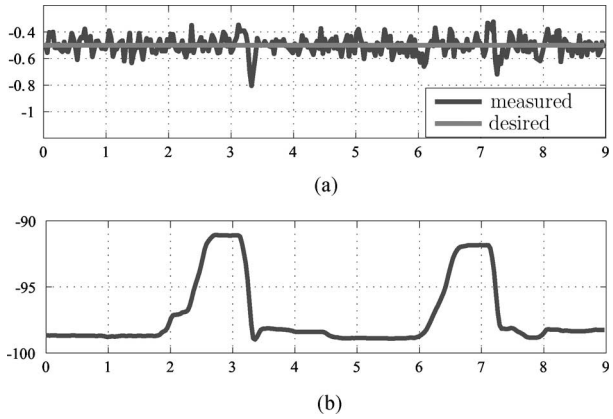

Fig. 14. Desired and measured contact force and the instrument position during *in vivo* force control experiment. (a) Desired and measured contact force ${}^4f_{dz}$ [N] versus time [s]. (b) Instrument position d_4 [mm] versus time [s].

with a desired contact force ${}^4f_{dz}$. The experimental results are given in Fig. 14. It can be observed in Fig. 14(a)) that the measured contact force ${}^4f_{e_z}$ is equal to the desired contact force ${}^4f_{d_z} = -0.5\,\mathrm{N}$, and that the contact is maintained throughout the breathing movement. However, a small disturbance is observed at $t = 3.1$ s and $t = 7.1$ s. This disturbance, which is rejected by the controller, is introduced by the dynamics of the patient's expiration movement. The position of the contact point during two breathing periods (given by the instrument position d_4) is reported in Fig. 14(b). Note that the dynamics of the inspiration movement (starts at $t = 2$ s and $t = 6$ s) is slower than the dynamics of the expiration movement (starts at $t = 3.1$ s and $t = 7.1$ s).

VII. Conclusion and Outlook

In this paper, a compact and lightweight robot for MIS was presented. This robot is mounted on the patient and offers a specialized kinematic design dedicated to MIS, which provides an invariant center at the fulcrum point.

In order to introduce force control into the OR, the measurement of manipulation forces inside the patient is a prerequisite. Therefore, a new trocar with an integrated force sensor allowing for the measurement of the contact forces was described. Although this sensor is placed outside the patient, neither friction inside the trocar nor the wrench between the trocar and the patient's skin deteriorate the measurements. Nevertheless, the gravity effect has to be considered in the measurements and, thus, has to be identified and compensated.

Experimental results on gravity compensation and force control were given, validating the chosen concepts.

Future work includes the setup of a force reflecting telemanipulation system for MIS, which will provide a realistic impression of the remote forces to the surgeon. Additionally, this robot is suited for comanipulation (i.e., soft robotics). Here, restricted motion along predefined trajectories and inside virtual walls bordering the work space will help to avoid unintentional damage of tissue.

References

[1] R. H. Taylor and D. Stoianovici, "Medical robotics in compter-integrated surgery," *IEEE Trans. Robot. Autom.*, vol. 19, no. 5, pp. 765–781, Oct. 2003.

[2] C. Wagner, N. Stylopoulos, and R. Howe, "The role of force feedback in surgery: Analysis of blunt dissection," in *Proc. 10th Int. Symp. Haptic Interfaces Virtual Environ. Teleoperator Syst.*, Orlando, FL, Mar. 2002, pp. 73–79.

[3] T. Ortmaier, "Motion compensation in minimally invasive robotic surgery," Ph.D. dissertation, Tech. Univ. Munich, Munich, Germany, 2003.

[4] J. M. Sackier and Y. Wang, Robotically assisted laparoscopic surgery: From concept to development*Computer-Integrated Surgery*. Cambridge, MA: MIT Press, 1995, pp. 577–580.

[5] G. Guthart and J. Salisbury, "The intuitive telesurgery system: Overview and application," in *Proc. IEEE Int. Conf. Robot. Autom.*, San Francisco, CA, Apr. 2000, pp. 618–621.

[6] H. Düpree, "Laprotek-master slave systeme in der Viszeralchirurgie," in *Proc. Jahrestagung der Deutschen Gesellschaft fur Comput.-und Roboterassistierte Chirurgie*, Nürnberg, Germany, Nov. 2003.

[7] M. C. Cavusoglu, W. Williams, F. Tendick, and S. Sastry, "Robotics for telesurgery: Second generation Berkeley/UCSF laparoscopic telesurgical workstation and looking towards the future applications," in *Proc. 39th Allerton Conf. Commun., Control Comput.*, Oct. 2001.

[8] D. Kwon, K. Woo, S. Song, W. Kim, and H. Cho, "Microsurgical telerobot system," in *Proc. IEEE/RSJ Int. Conf. Intell. Robots Control Syst.*, Victoria, BC, Canada, Oct. 1998, pp. 945–950.

[9] J. Rosen, B. Hannaford, M. MacFarlane, and M. Sinanan, "Force controlled and teleoperated endoscopic grasper for minimally invasive surgery—experimental performance evaluation," *IEEE Trans. Biomed. Eng.*, vol. 46, no. 10, pp. 1212–1221, Oct. 1999.

[10] T. Hu, A. Castellanos, G. Tholey, and J. Desai, "Real-time haptic feedback in laparoscopic tools for use in gastro-intestinal surgery," in *Proc. 5th Int. Med. Image Comput.-Comput. Assisted Intervention Conf.*, Tokyo, Japan, Sep. 2002, pp. 66–74.

[11] C. Kennedy, T. Hu, and J. Desai, "Combinig haptic and visual servoing for cardiothoracic surgery," in *Proc. IEEE Int. Conf. Robot. Autom.*, Washington, DC, May 2002, pp. 2106–2111.

[12] M. Tavakoli, R. Patel, and M. Moallem, "A force reflective master-slave system for minimally invasive surgery," in *Proc. IEEE/RSJ Int. Conf. Intell. Robots Syst.*, Las Vegas, NV, Oct. 2003, pp. 3077–3082.

[13] U. Seibold, B. Kuebler, H. Weiss, T. Ortmaier, and G. Hirzinger, "Sensorized and actuated instruments for minimally invasive robotic surgery," in *Proc. 4th Int. Conf. EuroHaptics*, Munich, Germany, Jun. 2004.

[14] U. Seibold and G. Hirzinger, "A 6-axis force/torque sensor design for haptic feedback in minimally invasive robotic surgery," in *Proc. 2nd VDE World Microtechnol. Congr.*, Munich, Germany, Oct. 2003.

[15] C. Preusche, T. Ortmaier, and G. Hirzinger, "Teleoperation concepts in minimally invasive surgery," *Control Eng. Pract. J.*, vol. 10, no. 11, pp. 1245–1250, Nov. 2002.

[16] G. Tholey, A. Pillarisetti, W. Green, and J. Desai, "Direct 3-D force measurement capability in an automated laparoscopic grasper," in *Proc. 4th Int. Conf. EuroHaptics*, Munich, Germany, Jun. 2004.

[17] P. J. Berkelman, L. L. Whitcomb, R. H. Taylor, and P. Jensen, "A miniature microsurgical instrument tip force sensor for enhanced force feedback during robot-assisted manipulation," *IEEE Trans. Robotics Autom.*, vol. 19, no. 5, pp. 917–922, Oct. 2003.

[18] A. Krupa, G. Morel, and M. et de Mathelin, "Achieving high precision laparoscopic manipulation using force feedback control," in *Proc. IEEE Int. Conf. Robotics Autom.*, Washington, DC, May 2002, pp. 1864–1869.

[19] T. Ortmaier and G. Hirzinger, "Cartesian control issues for minimally invasive robot surgery," in *Proc. IEEE/RSJ Int. Conf. Intell. Robots Syst.*, Takamatsu, Japan, Oct. 2000, pp. 565–571.

[20] M. Michelin, P. Poignet, and E. Dombre, "Geometrical control approaches for minimally invasive surgery," presented at the Workshop Med. Robotics Navig. Vis., Remagen, Germany, 2004.

[21] P. Berkelman, E. Boidard, P. Cinquin, and J. Troccaz, "LER: The light endoscope robot," in *Proc. IEEE/RSJ Int. Conf. Intell. Robots Syst.*, Las Vegas, NV, Oct. 2003, pp. 2835–2840.

[22] M. Lum, J. Rosen, M. Sinanan, and B. Hannaford, "Kinematic optimization of a spherical mechanism for a minimally invasive surgical robot," in *Proc. IEEE Int. Conf. Robotics Autom.*, New Orleans, LA, May 2004, pp. 829–834.

[23] G. Picod, A. Jambon, P. Dubois, and D. Vinatier, "Effect of laparoscopic trocar model on the quality of the movement: Experimental study of friction," *Gynecol. Obstet. Fertilite*, vol. 32, pp. 937–941, 2004.
[24] P. Dubois, Q. Thommen, and A. Jambon, "*In vivo measurement of surgical gestures*," *IEEE Trans. Biomed. Eng.*, vol. 49, no. 1, pp. 49–54, Jan. 2002.
[25] N. Zemiti, G. Morel, A. Micaelli, B. Cagneau, and D. Bellot, "A passive formulation of force control for kinematically constrained manipulators," in *Proc. IEEE Int. Conf. Robotics Autom.*, Orlando, FL, May 2006, pp. 2238–2243.

Nabil Zemiti received the B.Sc. degree in electronics engineering from the University of Science, Algiers, Algeria, in 2001, the M.Sc. degree in virtual reality and complex systems from the University of Versailles, Paris, France, in 2002, and the Ph.D. degree in robotics from the University of Paris 6, Paris, France, in 2005.

He is currently a Researcher at the Laboratoire de Robotique de Paris, Université Pierre et Marie Curie-Paris 6, Paris, France, where he is working on medical robotics and force-feedback control for robotic manipulators.

Guillaume Morel (M'97) received the Ph.D. degree from the University of Paris 6, Paris, France, in 1994.

He was a Postdoctoral Research Assistant in the Department of Mechanical Engineering, Massachusetts Institute of Technology, Cambridge, in 1996, and an Associate Professor at the University of Strasbourg, Illkirch, France, from 1997 to 2000. After a year spent as a Research Scientist for the French electric company (EDF), he joined the Laboratoire de Robotique de Paris, University of Paris 6, Paris, France. His research interests include sensor-based control of robots, with a particular focus on force-feedback control and visual servoing, and application of these techniques to medical robotics.

Tobias Ortmaier received the Diploma in electrical engineering and the Ph.D. degree in motion compensation in minimally invasive robotic surgery in 1998 and 2003, respectively, from the Technical University of Munich (TUM), Munich, Germany.

From November 2003 to October 2004, he was a Postdoctoral Fellow at the Robotics Laboratory of Paris, University of Paris 6, Paris, France. Since then he has been the Head of the Medical Robotics Group, Institute of Robotics and Mechatronics of the German Aerospace Center (DLR), Munich, Germany, as well as a Lecturer at the TUM for real-time computer vision for robotics. He is the author of more than 50 papers on robotics, mainly on medical robotics, telepresence, mechatronics, and computer vision.

Nicolas Bonnet received the M.D. degree in thoracic and cardiovascular surgery from the University of Paris 6, Paris, France, in 1997.

Since 1997 he has been with the Department of Cardiovascular Surgery, La Pitié Salpêtrière Assistance Publique des Hôpitaux de Paris, Paris, France. His research interests include clinical applications of robotic surgery.